Supporting Information

An effective strategy to improve contact selectivity in organic solar cells

Hui Jin[†], Xiaoyun Xu[†], Hongbo Wu[†], Zaifei Ma*[,†] and Zheng Tang*[,†]

[†] State Key Laboratory for Modification of Chemical Fibers and Polymer Materials, Center for Advanced Low-dimension Materials, College of Materials Science and Engineering, Donghua University, Shanghai 201620, China

Email: mazaifei@dhu.edu.cn, ztang@dhu.edu.cn

Table of contents

SI-1. Experimental Section

Materials and device fabrication:

PEDOT:PSS (CLEVIOS P VP AL 4083) was purchased from Heraeus, 1,8-diiodooctane (DIO) was purchased from Alfa Aesar, poly[(2,6-(4,8-bis(5-(2-ethylhexyl)thiophen-2-yl)-benzo[1,2-b:4,5-b′]dithiophene))-alt-(5,5-(1′,3′-di-2-thienyl-5′,7′-bis(2-ethylhexyl)benzo[1′,2′-c:4′,5′-c′]dithiophene-4,8-dione))] (PBDB-T), poly[(2,6-(4,8-bis(5-(2-ethylhexyl-3-fluoro)thiophen-2-yl)-benzo[1,2-b:4,5-b′]dithiophene))-alt-(5,5-(1′,3′-di-2-thienyl-5′,7′-bis(2-ethylhexyl)benzo[1′,2′-c:4′,5′-c′]dithiophene-4,8-dione)] (PM6), 3,9-bis(2-methylene-(3-(1,1-dicyanomethylene)-indanone))-5,5,11,11-tetrakis(4-hexylphenyl)-dithieno[2,3-d:2′,3′-d′]-s-indaceno[1,2-b:5,6-b′]dithiophene (ITIC), and PFN-Br were purchased from Solarmer Beijing, 2,2′-((2Z,2′Z)-((12,13-bis(2-ethylhexyl)-3,9-diundecyl-12,13-dihydro-[1,2,5]thiadiazolo[3,4-e]thieno[2,″30″:4′,5′]thieno[2′,3′:4,5]pyrrolo[3,2-g]thieno[2′,3′:4,5]thieno[3,2-b]indole-2,10-diyl)bis(methanylylidene))bis(5,6-difluoro-3-oxo-2,3-dihydro-1H-indene-2,1-diylidene))dimalononitrile (Y6), [6,6]-phenyl-C_{71}-butyric acid methyl ester ($PC_{71}BM$) were purchased from Zhi-yan Company.

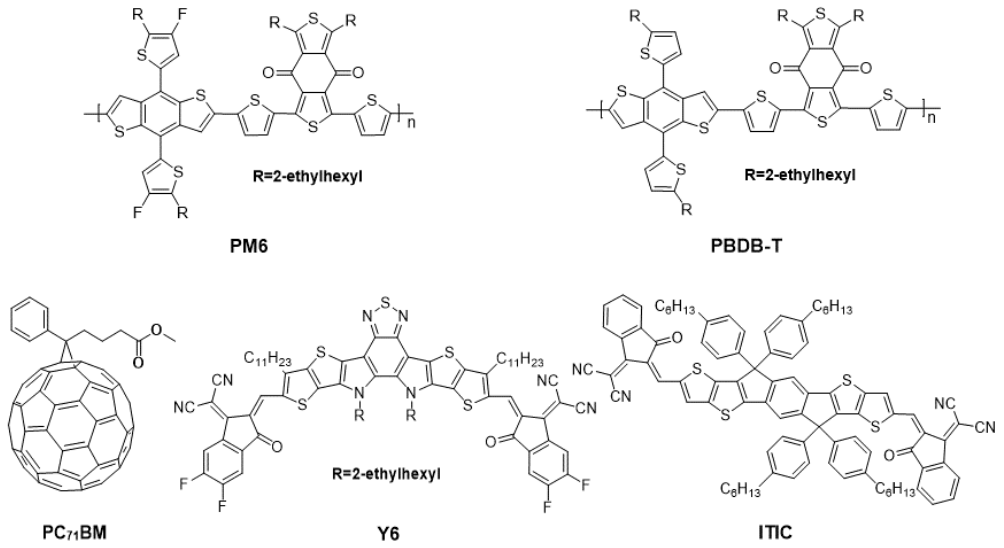

Scheme S1. Chemical structures for PM6, PBDB-T, $PC_{71}BM$, Y6 and ITIC.

Solution-processed bulk-heterojunction solar cells were fabricated as follows: ITO-coated glass substrates were sonicated in detergent, distilled water, acetone, isopropyl alcohol, and then ethyl alcohol. PEDOT:PSS layers were spin-coated on top of the substrates at 5000 rpm for 50 s. The substrates were subsequently dried at 150℃ for 20 min on a hotplate and then transferred to a nitrogen filled glovebox. The thickness of PEDOT:PSS layers was about 30 nm. The solutions of PBDB-T:$PC_{71}BM$ and PBDB-T:ITIC were prepared using chlorobenzene (CB) as solvent. The donor:acceptor (D:A) weight ratio was 1:1, and the solution concentration was 18 $mg \cdot ml^{-1}$. The active layers were spin-coated at 3000 rpm for 40 s on top the PEDOT:PSS coated substrates. Then the active layer films were annealed at 120℃ for 10 min. The thicknesses of the active layers were about 90 nm, determined by the profilometer (KLA P-7 Stylus Profiler). The solution of PM6:$PC_{71}BM$ was prepared using CB as solvent. The D:A weight ratio was 1:1, and the solution concentration was 20 $mg \cdot ml^{-1}$. The solution was stirred at 50 °C for about 10 hours. The PM6:$PC_{71}BM$ active layer was spin-coated at 3000 rpm for 40 s onto the PEDOT:PSS layer, and the film was annealed on a hotplate at 100 ℃ for 10 min to remove the residual solvent. The thickness of the active layers was 100 nm. The solution of PM6:Y6 was prepared using chloroform (CF) as solvent. The D:A weight ratio was 1:1, and the solution concentration was 16 $mg \cdot ml^{-1}$. The solution was stirred at 40°C for about 5 hours. The PM6:Y6 active layer was spin-coated at 3500 rpm for 40 s, and the film was annealed at 100 ℃ for 5 min. The thickness of the active layer was about 120 nm. The solutions of PM6:Y6:$PC_{71}BM$ with different $PC_{71}BM$ content were prepared using chloroform (CF). The concentration of the solutions was 16 $mg \cdot ml^{-1}$. The solutions were stirred at 50 °C for about 6 hours. The PM6:Y6:$PC_{71}BM$ films were prepared by spin-coating at 3500 rpm for 40 s, and they were annealed at 100 ℃ for 5 min. The solutions of PBDB-T:ITIC:$PC_{71}BM$ with different $PC_{71}BM$ content were prepared using CB. The concentration of the solutions was 18 $mg \cdot ml^{-1}$. The solutions were stirred at 90 °C for about 8 hours. The PBDB-T:ITIC:$PC_{71}BM$ active layers were spin-coated at 3000 rpm for 40 s, and they were annealed at 120℃ for 10 min. For constructing the DIO treated solar cells, the active layer, before being

removed from the spin-coater, was soaked by the DIO solution (80 μl). The solution was prepared by mixing DIO with IPA. Then, the DIO solution was removed from the active layer by the spin-coater spinning at 5000 rpm. The active layer was transferred onto a hotplate and annealed at 100 ℃ for 5 min. Finally, a 100 nm Ag electrode was deposited by thermal evaporation under a vacuum pressure of $1x10^{-6}$ mbar. The active area of the solar cells was 0.04 cm^2.

Device characterization:

J-V curves of the solar cells were measured under a simulated AM 1.5 G illumination (100 $mW \cdot cm^{-2}$) with a solar simulator (Newport Oriel VeraSol-2™ Class AAA), calibrated with a set of low-pass optical filters and a standard Si photo diode. The J_{sc} of the solar cells were calibrated by EQE measurements.

EQE spectra of OSCs were measured with a halogen lamp (LSH-75, 250W, Newport), a monochromator (CS260-RG-3-MC-A, Newport), an optical chopper with a frequency of 173 Hz (3502 Optical Chopper, Newport). A second halogen lamp was used to provide bias illumination (100 mW/cm^2). The photocurrent signals were recorded using a front-end current amplifier (SR570, Stanford Instrument) and a lock-in amplifier (SR830, Stanford Instrument). A focus lens and an optical aperture were used to reduce the size of the illuminated area to 0.5 mm^2.

EQE_{EL} of the solar cells were determined by using a digital source meter (Keithley 2400), to inject electric current into the solar cells, and a picoammeters (Keithley 6482) collected to a Si diode, to measure emitted photons from the solar cells.

EL spectra of OSCs were measured by using a source meter (Keithley 2400) to inject electric current into the OSCs, and emitted photons were collected by an optical fiber and recorded by a fluorescence spectrometer (KYMERA-3281-B2, Andor), a Si EMCCD camera (DU970P-BVF, Andor), and an InGaAs camera (DU491A-1.7, Andor).

PL spectra of the active layers were measured with a laser (SuperK EXU-6, NKT photonics) and narrowband filters (LLTF Contrast SR-VIS-HP8, NKT photonics) as the light source. The excitation wavelength was 480 nm. Photons emitted from the thin films were collected and recorded by the same setup used for the EL spectra

measurements.

Transient photocurrent *vs* voltage curves of the solar cells were measured using a green LED. The V_{oc} of the solar cell under the LED illumination is close to that under the simulated AM1.5G illumination. An oscilloscope (MDO4104C, Tektronix) was used to record the transient photocurrent signals. A Keithley 2400 is used to apply voltage to the solar cell. The impact of series resistance in the electrodes of the solar cells is minimized using a "4-point" method: the sensing of the voltage applied to the active layer of the solar cell is done via connecting an additional set of anode and cathode terminals to a voltmeter.

AFM images were measured using MFP-3D-BIO™, Asylum Research, in a tapping-Mode.

XPS spectra were measured using Escalab 250Xi, Thermo Scientific, using 200W monochromated Al Ka radiation in an ultra-high vacuum with a pressure of $1x10^{-9}$ mbar.

SI-2. Performance of the solar cells based on PM6:$PC_{71}BM$

Table S1. Summary of the photovoltaic (PV) parameters for the solar cells based on PM6:$PC_{71}BM$.

Active layer		J_{sc} (mA/cm^2)	V_{oc} (V)	*FF* (%)	*PCE* (%)
PM6:$PC_{71}BM$	w/o DIO	12.5±0.3	0.83±0.01	57±2	5.93 ± 0.10
	w/ DIO	12.3±0.3	0.90±0.01	59±3	6.49 ± 0.34

Table S2. Summary of PV performance parameters of the solar cells based on PM6:$PC_{71}BM$ modified by DIO with different DIO (in IPA) concentrations. The active layers are soaked in DIO for 1min.

Active layer	DIO (vol%)	J_{sc} (mA/cm^2)	V_{oc} (V)	*FF* (%)	*PCE* (%)
PM6:$PC_{71}BM$	0.1	12.3±0.5	0.86±0.01	59±2	6.28 ±0.14
	0.01	12.4±0.3	0.88±0.01	59±3	6.45 ±0.14
	0.001	12.4±0.5	0.86±0.01	58±3	6.20 ±0.23
	0	12.2±0.4	0.84±0.01	57±2	5.90 ±0.18

Table S3. Summary of the PV parameters of the solar cells based on PM6:$PC_{71}BM$ modified by DIO with different soaking time. The concentration of DIO (in IPA) is 0.01 (vol%).

Active layer	Soaking time (min)	J_{sc} (mA/cm^2)	V_{oc} (V)	*FF* (%)	*PCE* (%)
PM6:$PC_{71}BM$	0	12.5±0.3	0.83±0.01	57±2	5.93 ±0.10
	1	12.4±0.3	0.88±0.01	59±3	6.45 ±0.14
	3	12.4±0.5	0.89±0.01	59±3	6.43 ±0.19
	5	12.3±0.3	0.90±0.01	59±3	6.49 ±0.34

Table S4. Summary of PV parameters of the solar cells based on PM6:$PC_{71}BM$, unmodified and modified by neat IPA.

Active layer	Soaking time (min)	J_{sc} (mA/cm^2)	V_{oc} (V)	*FF* (%)	*PCE* (%)
PM6:$PC_{71}BM$	0	12.5±0.3	0.83±0.01	57±2	5.93±0.10
	5	11.9±0.3	0.85±0.01	58±2	5.86±0.17

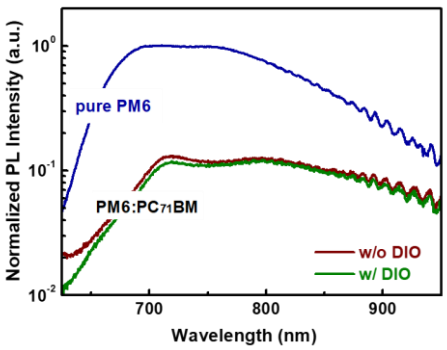

Figure S1. PL spectra for the pure PM6 film and the blend films based on PM6:$PC_{71}BM$ with and without the DIO modification. The excitation wavelength used is 480 nm.

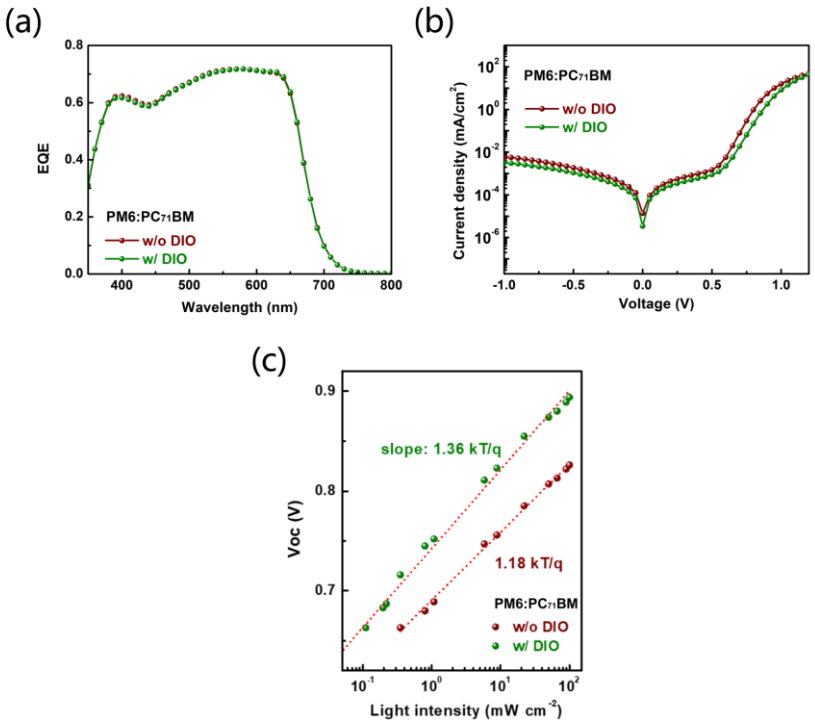

Figure S2. (a) EQE spectra, (b) dark *J-V* curves, and (c) V_{oc} *vs* light intensity curves for the solar cells based on PM6:$PC_{71}BM$ with and without the DIO modification.

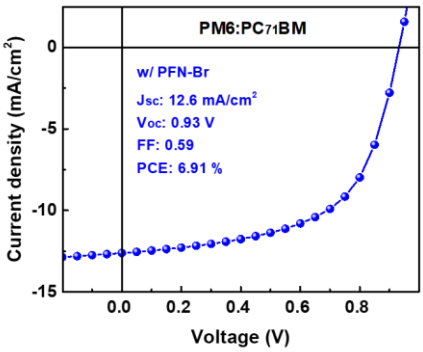

Figure S3. The JV curve and the photovoltage performance parameters for the standard solar cell based on PM6:$PC_{71}BM$.

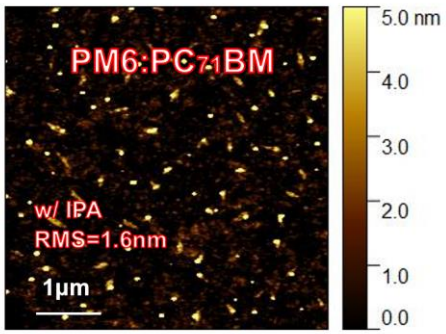

Figure S4. AFM images of the active layers based on PM6:$PC_{71}BM$ treated by neat IPA.

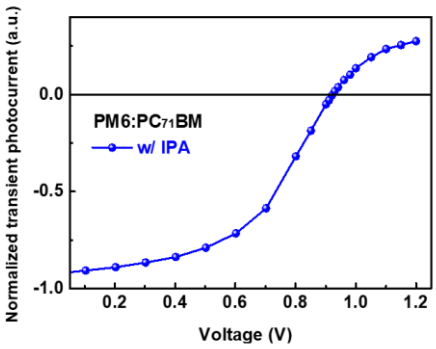

Figure S5. Transient photocurrent as a function of applied voltage for the solar cell based on PM6:$PC_{71}BM$ treated by neat IPA.

SI-3. Determination of the CT state properties of OSCs

The tails of the EQE spectra of the solar cell are measured by a sensitive EQE setup, which consists of a halogen lamp, a monochromator, a current amplifier and a lock-in amplifier. A set of long pass filters were used to make sure that light reaching the solar cells is truly monochromatic. In addition, EL spectra of the solar cells are also measured. The measured EL spectra were converted to absorption spectra, using the reciprocal relation (*Phys. Rev. B*, **2007**, 76, 085303). This further extend the tails of the EQE spectra.

To determine the CT state properties of the BHJ solar cells, the tails of the EQE spectra, corresponding to CT absorption, are fitted by the equation derived in the framework of Marcus theory (*J. Phys. Chem.*, **1989**, 93, 3078; *Phys. Rev. B*, **2010**, 81, 125204),

$$EQE(E) = \frac{fE}{\sqrt{4\pi\lambda kT}} exp\ (-\frac{(E_{CT} + \lambda - E)^2}{4\lambda kT})$$

where E is photon energy, λ is reorganization energy, k is the Boltzmann constant, T is temperature, and f is a prefactor related to the device internal quantum efficiency and the absorption oscillator strength of the solar cell.

For the solar cells based on the PM6:$PC_{71}BM$ and PBDB-T:$PC_{71}BM$, the fittings are easily done, because the peak of CT absorption is at a much lower energy, compared to the absorption spectrum of the donor or the acceptor. However, for the solar cells based on the binary PBDB-T:ITIC or the PBDB-T:ITIC:$PC_{71}BM$ ternary systems, the CT absorption peak is very close to the acceptor absorption. To avoid an arbitrary fitting to the low energy part of the EQE spectra, we introduce two boundary conditions for the fitting process (*J. Mater. Chem. A*, **2021**, DOI:10.1039/D1TA00576F). More specifically, we first use E_{CT} as the effective energy of bandgap in the Shockley-Queisser theory, and calculate the lower limit for the radiative recombination voltage loss ($\Delta V_{r,sq}$). And then, a set of fixed f values in the range between 0.0001 to 0.1 are used for the fitting process. This allows us to obtain a set of fit parameters. Subsequently,

we use the fit results for E_{CT} to calculate ΔV_r ($\Delta V_r = E_{CT} - V_{oc} - \Delta V_{nr}$), which is then compared to $\Delta V_{r,sq}$ for the determination of the lower limit for *f*, and thus, the lower limit for E_{CT} and λ. For the determination of the upper limit for the CT state related parameters, we use the value of *f* that gives rises to a peak EQE value for the CT absorption approximately ten times lower than the peak of the EQE contributed by the pristine donor or acceptor absorption. This is because of the fact that the highest CT state absorption coefficient in OSCs has been found for the biomolecular crystal system of PBTTT:$PC_{71}BM$ (*Adv. Mater.*, **2017**, 29, 1702184.), and for this system, the EQE value at the peak of CT state absorption is less than 5%, compared to the peak EQE of the pristine material. Note that for the solar cells based on PM6:$PC_{71}BM$, PBDB-T:$PC_{71}BM$, PBDB-T:ITIC, and the ternary PBDB-T:ITIC:$PC_{71}BM$ blend studied in this work, the difference between the upper and the lower limit for E_{CT} is less than 0.05 eV. For the solar cells based on PM6:Y6 or PM6:Y6:$PC_{71}BM$, we are unable to determine the CT state properties from the sensitive EQE spectra, because the CT absorption peak is too close to the acceptor absorption.

SI-4. Performance of the solar cells based on PBDB-T:$PC_{71}BM$

We also constructed solar cells using the blend of PBDB-T:$PC_{71}BM$ as the photoactive materials. It is noted that $PC_{71}BM$ molecules are extracted to the surface of the active layer after the DIO modification, according to the AFM images (Figure S6a). XPS measurements (Figure S6b) reveal that the S2p signal, originating from the donor of the active layer, reduces after the DIO modification, suggesting an increased $PC_{71}BM$ content at the surface of the active layer. From the *J-V* curves (Figure S7a) and the photovoltaic performance parameters of the solar cells are listed in Table S5, we find that J_{sc} of the solar cells with and without the DIO modification are the same, since the DIO modification does not alter the bulk property of the active layer. Indeed, E_{CT} (Figure S7b), PLQE (Figure S7c), and EQE (Figure S7d) of the solar cell are barely affected by the DIO modification.

However, V_{oc} of the modified solar cell (0.80 V) is considerably higher than that of the unmodified solar cell (0.74 V). The increased V_{oc} is ascribed to the reduced ΔV_{nr}, a result of increased EQE_{EL} (Figure S7g). Also, from the transient photocurrent-voltage measurements (Figure S8a and S8b), we note that the contact selectivity of the solar cell is improved after the DIO modification.

These results confirm that the DIO modification can generally lead to the formation of a dense $PC_{71}BM$ interlayer at the surface of the binary polymer:fullerene active layer, improving electron selectivity of the cathode, and thus, reducing voltage loss and improving the performance of the solar cell.

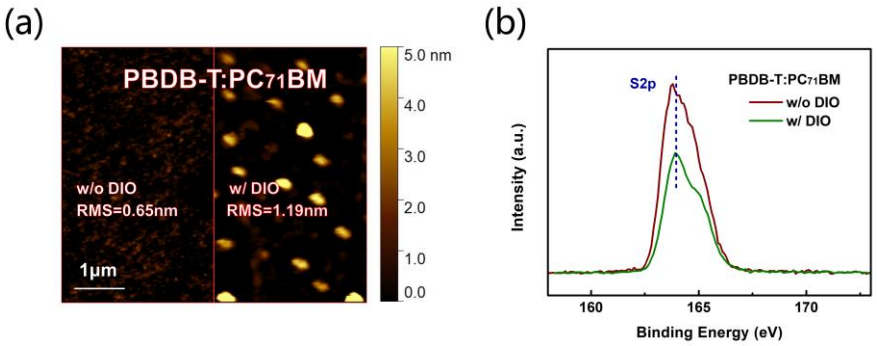

Figure S6. (a) AFM images and (b) XPS of the active layers based on PBDB-T:$PC_{71}BM$ with and without the DIO treatment.

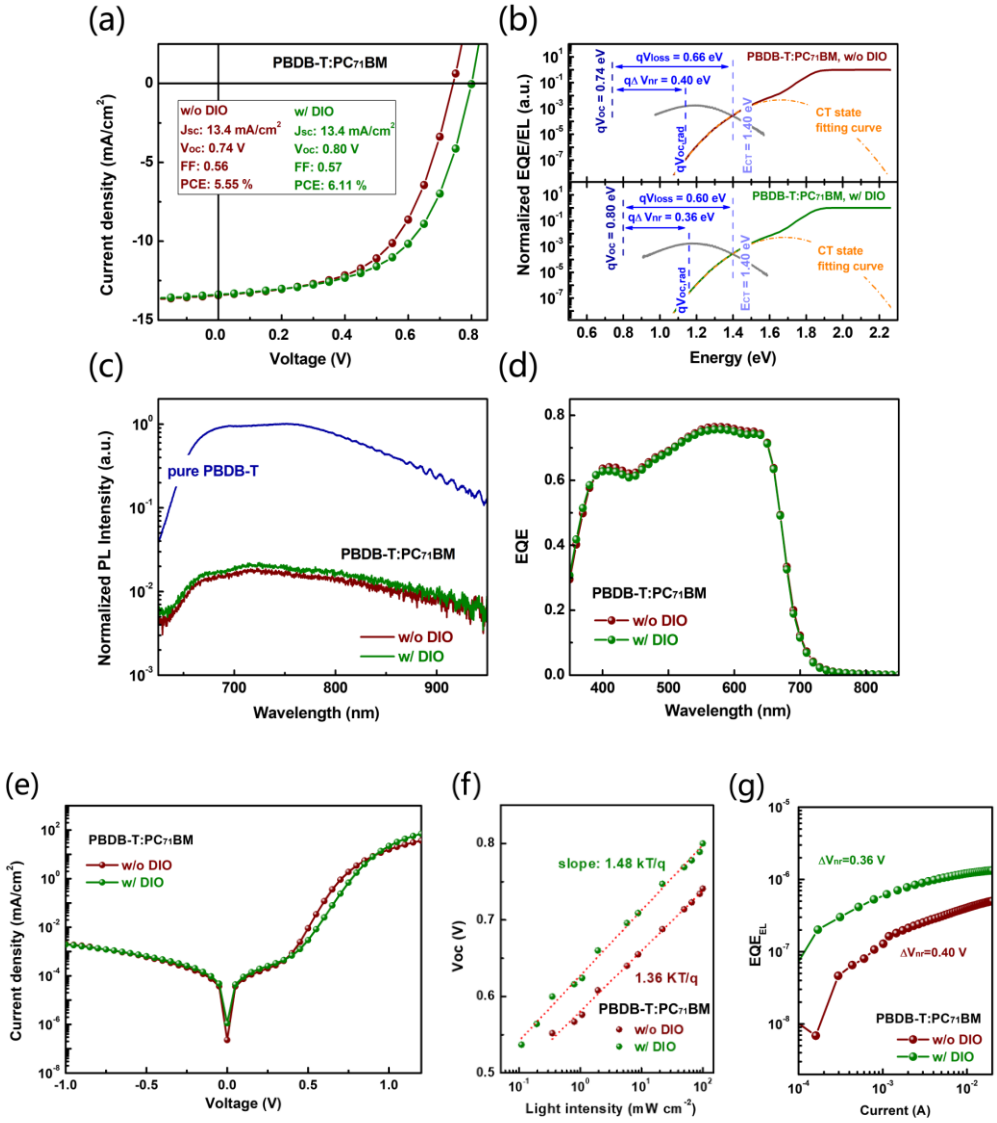

Figure S7. (a) *J-V* curves, (b) sensitive EQE and EL spectra, (c) PL spectra, (d) EQE spectra, (e) dark *J-V* curves, (f) V_{oc} *vs* light intensity curves for the solar cells based on PBDB-T:$PC_{71}BM$ with and without the DIO modification, and (g) EQE_{EL} of the solar cells based on PBDB-T:$PC_{71}BM$.

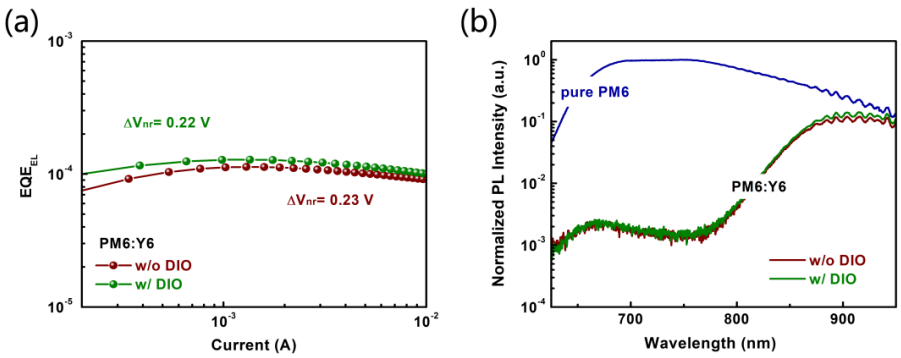

Figure S8. (a) Transient photocurrent as a function of applied voltage, and (b) the first derivative of the transient photocurrent *versus* voltage curves for the solar cells with and without the DIO modification.

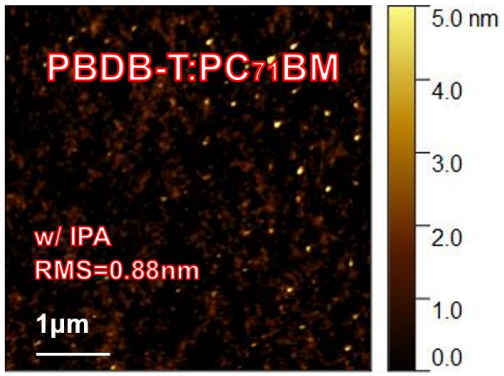

Figure S9. AFM images of the active layers based on PBDB-T:$PC_{71}BM$ treated by neat IPA.

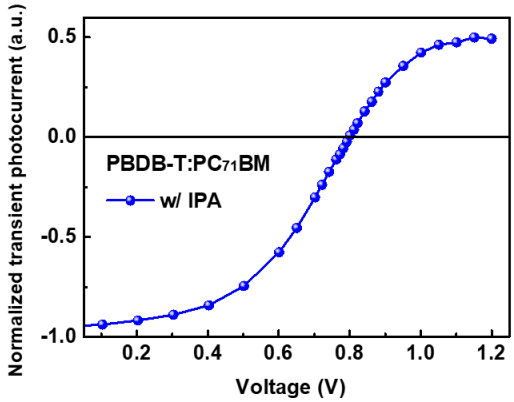

Figure S10. Transient photocurrent as a function of applied voltage for the solar cell based on PBDB-T:$PC_{71}BM$ treated by neat IPA.

Table S5. Summary of the PV parameters of the solar cells based on PBDB-T:$PC_{71}BM$ modified by different concentrations of DIO and different soaking times.

Active layer	DIO ratio (vol%)	Soaking time (min)	J_{sc} (mA/cm^2)	V_{oc} (V)	*FF* (%)	*PCE* (%)
PBDB-T:$PC_{71}BM$	10	1	5.6±1.8	0.67±0.01	51±3	1.88 ±0.43
	1	1	12.3±0.2	0.72±0.01	57±3	4.98 ±0.22
	0.1	1	13.1±0.2	0.77±0.01	55±2	5.52 ±0.16
	0.01	1	13.1±0.2	0.78±0.01	56±1	5.75 ±0.09
	0.01	3	13.1±0.3	0.78±0.01	56±1	5.69 ±0.14
	0.01	5	13.2±0.3	0.79±0.01	57±2	5.94 ±0.17
	0.001	1	13.0±0.2	0.77±0.01	57±1	5.69 ±0.10
	0	1	12.9±0.2	0.75±0.01	56±1	5.40 ±0.19
	0	5	12.9±0.3	0.75±0.01	56±1	5.44 ±0.20
	/	0	13.1±0.3	0.74±0.01	56±2	5.40 ±0.15

SI-5. Performance of the solar cells based on PM6:Y6

Table S6. Summary of the PV parameters of the solar cells based on PM6:Y6 modified by DIO with different soaking times. The concentration of DIO (in IPA) is 0.01 (vol%).

Active layer	Soaking time (min)	J_{sc} (mA/cm^2)	V_{oc} (V)	*FF* (%)	*PCE* (%)
PM6:Y6	0	23.9±0.3	0.81±0.01	57±2	10.96 ±0.32
	1	23.8±0.4	0.81±0.01	57±3	10.95 ±0.57
	5	23.8±0.5	0.82±0.01	58±4	11.24 ±0.23

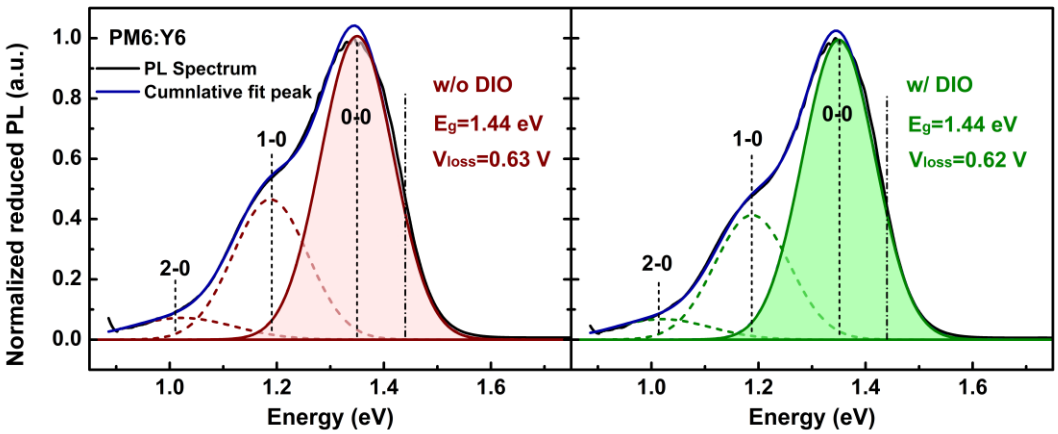

Figure S11. Determination of V_{loss} in the solar cells based on PM6:Y6 with and without the DIO modification. Because the energy range of CT state absorption for the solar cells based on PM6:Y6 is extremely close to that of the pristine Y6 absorption. Determination of E_{CT} is not possible with the sensitive EQE measurements (*ACS Energy Lett.*, **2021**, 6, 557). Therefore, we measure E_g of the blend active layer, using the method reported in the literature (*Sustain. Energy Fuels*, **2018**, 2, 538) and we determine V_{loss}, using the equation $V_{loss} = E_g/q - V_{oc}$.

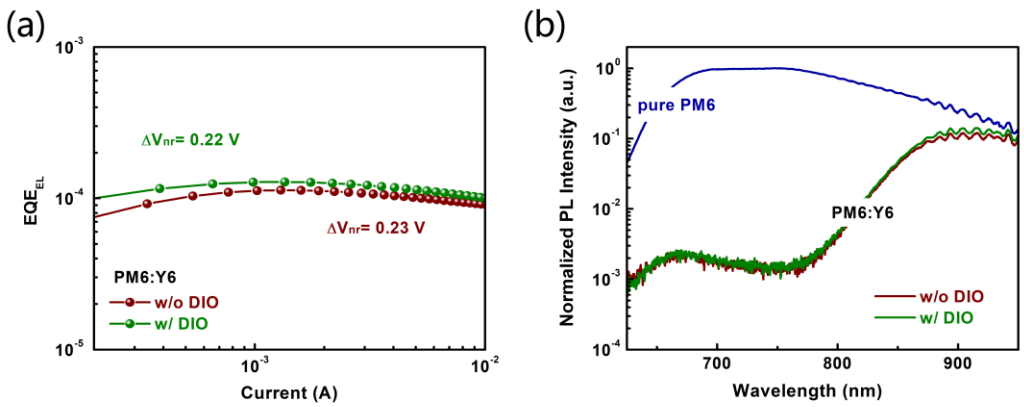

Figure S12. (a) EQE_{EL} and (b) PL spectra of the solar cells based on PM6:Y6 with and without the DIO modification.

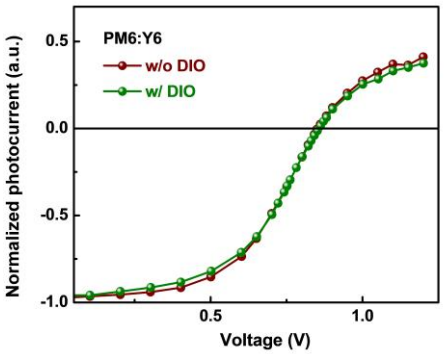

Figure S13. Transient photocurrent as a function applied voltage for the solar cells with and without the DIO modification.

SI-6. Performance of the solar cells based on PBDB-T:ITIC

Non-fullerene solar cells based on PBDB-T:ITIC are also constructed to evaluate the impact of the DIO modification on the device performance. The processing conditions used for the optimization of the device performance are summarized in Table S7. AFM images (Figure S14a) suggest that the DIO modification has no impact on the surface properties of the active layer. Also, the CT state properties (Figure S14b) and PLQEs of the active layers (Figure S14c) are the same for the solar cells with and without after the DIO modification. Therefore, the DIO modification does not increase the EQE_{EL} (Figure S14d), and the contact selectivity of the solar cell does not increase after the DIO modification (Figure S15a). The overall performance of the solar cells is poor, with or without the DIO modification, due to high V_{loss}, leading to low V_{oc} (Figure S15b).

Table S7. Summary of the PV parameters of the solar cells based on PBDB-T:ITIC modified by DIO with different soaking times. The concentration of DIO (in IPA) is 0.01 (vol%).

Active layer	Soaking time (min)	J_{sc} (mA/cm^2)	V_{oc} (V)	*FF*(%)	*PCE* (%)
PBDB-T: ITIC	0	15.5±0.4	0.80±0.01	52±2	6.52±0.18
	1	15.4±0.2	0.81±0.01	54±3	6.70±0.19
	5	15.4±0.2	0.82±0.01	53±3	6.66±0.25

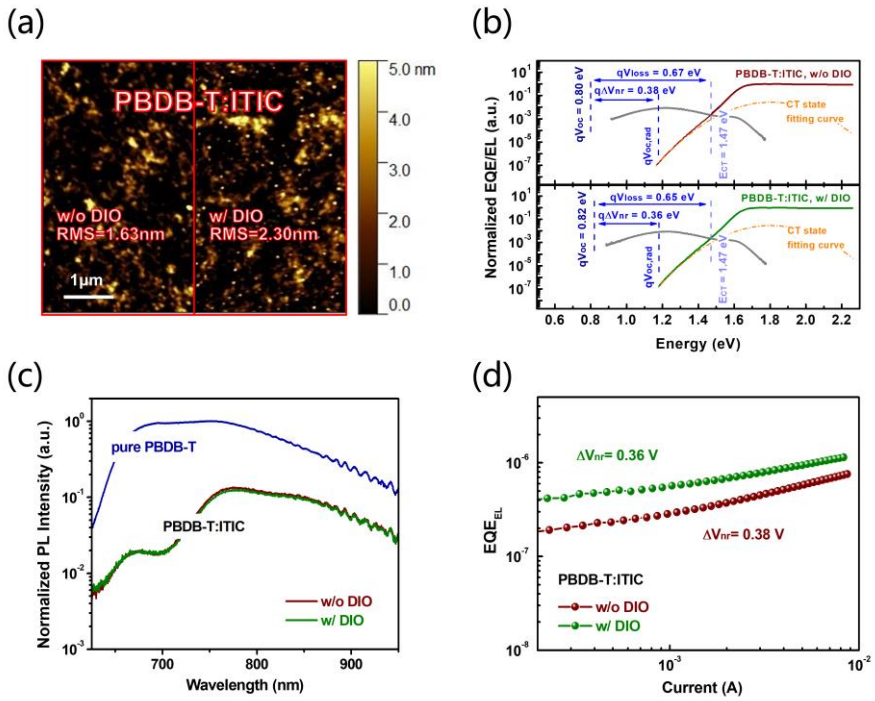

Figure S14. (a) AFM images, (b) sensitive EQE and EL spectra, (c) PL spectra and (d) EQE_{EL} for the solar cells based on PBDB-T:ITIC.

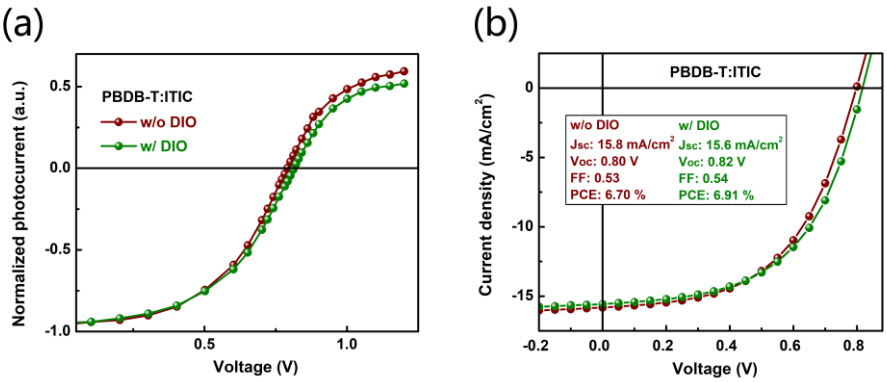

Figure S15. (a) Transient photocurrent as a function applied voltage, and (b) *J-V* curves for the solar cells with and without the DIO modification.

SI-7. Performance of the ternary OSCs based on PM6:Y6:$PC_{71}BM$

Table S8. Summary of the PV parameters of the ternary solar cells based on PM6:Y6:$PC_{71}BM$, with and without the DIO modification. For the modified solar cells, the active layers are treated by DIO with a concentration of 0.01 vol% in IPA for 5 min. Note that the content of $PC_{71}BM$ is the mass ratio between $PC_{71}BM$ and PM6:Y6.

$PC_{71}BM$ content (%)	Treatment	J_{sc} (mA/cm^2)	V_{oc} (V)	*FF*(%)	*PCE* (%)
0	w/o DIO	23.9±0.3	0.81±0.01	57±2	10.96±0.30
	w/ DIO	23.8±0.5	0.82±0.01	58±4	11.24±0.45
5	w/o DIO	23.8±0.2	0.81±0.01	56±2	10.65±0.29
	w/ DIO	23.7±0.3	0.82±0.01	59±2	11.52±0.37
10	w/o DIO	23.8±0.4	0.81±0.01	56±3	10.69±0.59
	w/ DIO	23.6±0.4	0.83±0.01	60±3	11.82±0.58
20	w/o DIO	23.4±0.4	0.81±0.01	57±2	10.78±0.36
	w/ DIO	23.3±0.3	0.84±0.01	59±2	11.46±0.27

SI-8. Performance of the ternary OSCs based on PBDB-T:ITIC:$PC_{71}BM$

Optimization of the ternary solar cells based on PBDB-T:ITIC:$PC_{71}BM$ is provided in Table S9. The *J-V* curves of the optimized ternary solar cells with $PC_{71}BM$ content of 20 wt%, with and without the DIO treatment, are shown in Figure S16a, and the AFM images are shown in Figure S16b. From the AFM images, we note that $PC_{71}BM$ is extracted to the surface of the ternary blend active layer after the DIO modification. Accordingly, V_{OC} of the solar cell is increased from 0.80 to 0.86 V, after the DIO modification, due to the increased device EQE_{EL} (Figure S16c). The contact selectivity is indeed improved for the ternary solar cell after the DIO modification (Figure S17a and S17b).

Table S9. Summary of PV parameters of the ternary solar cells based on PBDB-T:ITIC:$PC_{71}BM$, with different contents of $PC_{71}BM$, with and without the DIO modification. For the modified solar cells, the active layers are treated by DIO with a concentration of 0.01 vol% in IPA for 5 min. Note that the content of $PC_{71}BM$ is the mass ratio between $PC_{71}BM$ and PBDB-T:ITIC.

$PC_{71}BM$ content (%)	Treatment	J_{sc} (mA/cm^2)	V_{oc} (V)	*FF*(%)	*PCE* [a](%)
0	w/o DIO	15.5±0.4	0.80±0.01	52±2	6.52±0.21
	w/ DIO	15.4±0.2	0.82±0.01	53±3	6.65±0.24
5	w/o DIO	15.7±0.2	0.80±0.01	51±1	6.42±0.19
	w/ DIO	15.6±0.1	0.82±0.01	52±1	6.69±0.14
10	w/o DIO	16.0±0.3	0.79±0.01	52±1	6.58±0.09
	w/ DIO	16.0±0.1	0.84±0.01	54±1	7.16±0.10
20	w/o DIO	15.7±0.1	0.80±0.01	54±1	6.73±0.10
	w/ DIO	15.7±0.2	0.86±0.01	56±1	7.50±0.20
40	w/o DIO	15.1±0.3	0.80±0.01	54±2	6.54±0.13
	w/ DIO	15.0±0.3	0.86±0.01	55±3	7.09±0.32

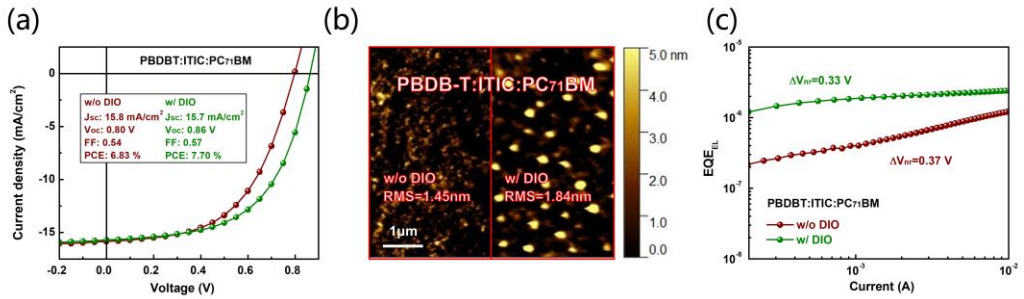

Figure S16. (a) *J-V* curves, (b) AFM images, and (c) EQE_{EL} for the ternary solar cells based on PBDB-T:ITIC:$PC_{71}BM$ with and without the DIO modification.

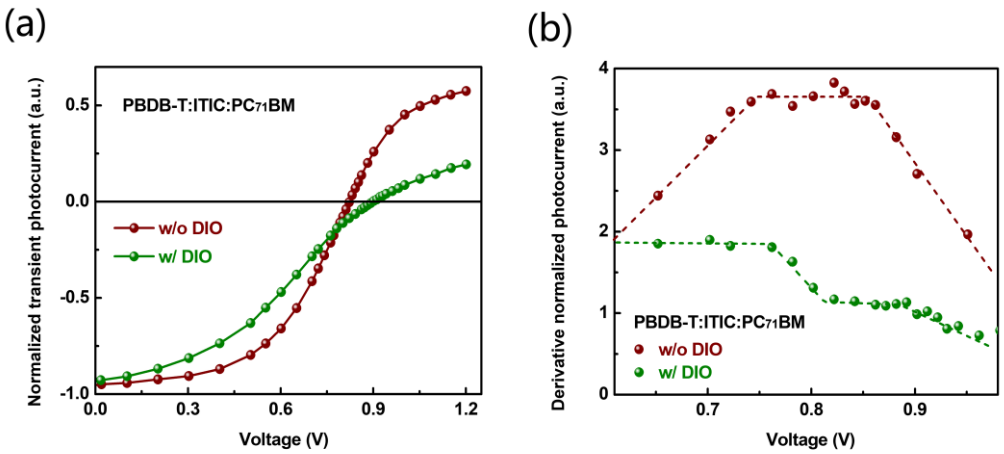

Figure S17. (a) Transient photocurrent as a function of applied voltage, and (b) the first derivative of the transient photocurrent *versus* voltage curves for the ternary solar cells with and without the DIO modification.